INTERACTION OF A FINITE-SIZED PARTICLE WITH WALL TURBULENCE

Lanying Zeng, S. Balachandar
Department of Theoretical and Applied Mechanics,
University of Illinois at Urbana-Champaign
Urbana, IL 61801, USA
lzeng@uiuc.edu, s-bala@uiuc.edu

Paul Fischer
Mathematics and Computer Science Division,
Argonne National Laboratory
Argonne, IL 60439, USA
fischer@mcs.anl.gov

Fady Najjar
Center for Simulation of Advanced Rockets,
University of Illinois at Urbana-Champaign
Urbana, IL 61801, USA
fnajjar@galileo.cse.uiuc.edu

ABSTRACT

Reliable information on forces on a finite-sized particle in a turbulent boundary layer is lacking. For lack of such knowledge we continue to use standard drag and lift correlations developed for a uniform flow to predict the drag and lift forces. Here we consider direct numerical simulations of a turbulent channel flow over a finite-sized particle. All relevant length and time scales of turbulence, attached boundary layers on the particles, and particle wakes will be faithfully resolved, and thus we consider fully resolved *genuine* direct numerical simulations. The results from the direct numerical simulation are compared with the corresponding predictions based on standard drag relation.

INTRODUCTION

Dispersed multiphase flows are common in many engineering and environmental applications. The essence of dispersed multiphase flow is at the interface between the phases, in terms of deformation, mass, momentum and energy transfer. Accurate accounting of these inter-facial processes is essential to both the Eulerian-Lagrangian and Eulerian-Eulerian approaches. For example, the hydrodynamic force on the dispersed phase controls critical processes such as dispersion, preferential accumulation, deposition, resuspension, collision & agglomeration, and deformation & breakup. The particles in turn modulate the carrier phase through back-coupling of mass, momentum and energy.

In macroscale formulations of multiphase flow, interface coupling is taken into account in terms of correlations for drag coefficient (Schiller and Naumann 1933) , lift coefficient (Mei 1992, Dandy and Dwyer 1990) and heat transfer (Ranz and Marshall 1952). Other correlations that attempt to account for additional effects, such as compressibility, evaporation, etc, can be found in recent books (Crowe et al. 1998, Sirignano 1999). Such empirical correlations are obtained for simple ambient flow conditions, when the scales of carrier phase flow are much larger than the scales of dispersed phase. However, their accuracy is not guaranteed when used beyond their range of validity, especially for *finite-sized* particles, defined as particles whose size is comparable or larger than the scales of carrier phase.

A quick survey of recent literature shows several hundred references to the above correlations attesting for their popularity and widespread use. In many of these applications there is significant turbulence at the scale of the particles and the wall effects could not be ignored. The usage of the correlations under such conditions is clearly outside the range of applicability originally intended. Nevertheless, their use is justified for the simple reason that there is nothing better available. Without further confidence in the applicability of these correlations, design of multiphase systems must use large safety factors and therefore cannot be properly optimized. The available experiments lack consensus and suggest widely varying effect of freestream turbulence, anywhere from substantial increase to dramatic reduction of mean drag (Brucato et al. 1998, Gore and Crowe 1990, Wu and Faeth 1994a). Recent computations have somewhat clarified the picture (Bagchi and Balachandar 2004). Based on these results freestream isotropic turbulence has little systematic effect on time-averaged mean drag. However, it is hard to accurately predict the instantaneous force fluctuations with the standard correlation. Especially, for particles of size larger than Kolmogorov scale the departure from prediction is quite significant. We believe freestream turbulence induced vortex shedding is responsible for such stochastic behavior. When viewed at the macroscale, the interface coupling for finite-sized particles is fundamentally stochastic. The correlations in common use are deterministic in nature and therefore can at best only hope to capture the mean behavior.

Experimental results (Fessler et al. 1994, Kaftori et al. 1995, Young and Hanratty 1991) suggest an even more complex interaction between particles and wall turbulence. Here we report on results obtained from direct numerical simulations (DNS) of a finite-sized particle embedded in a fully developed turbulent channel flow. These are *fully resolved* numerical simulations, where in addition to resolving the wide range of length and time scales associated with wall turbulence, all the length and time scales associated with the particles and the small-scale flow features generated by them are fully resolved.

The results from such fundamental simulations will provide definitive answers to applicability of commonly used drag and lift correlations. In particular, we hope to answer how small a particle needs to be, compared to Kolmogorov scale, for it to be treated as a point particle. For larger particles, the simulations will provide detailed information on the stochastic nature of interface momentum coupling. The simulations also provide detailed statistical information on the back effect of particles on carrier phase turbulence. Here however, we will limit attention to only the effect of wall turbulence on forces on the particle.

NUMERICAL METHODOLOGY

We consider a rigid stationary sphere of diameter, d, located within a turbulent channel flow. The particle is placed at a distance y_p from the lower wall and the channel turbulence is characterized by Reynolds number based on channel half height (H) and friction velocity (u_τ) of $Re_\tau = Hu_\tau/\nu = 178.12$. The nondimensional diameter of the particle in wall units ($d_+ = du_\tau/\nu$) is chosen to be 17.81 and the distance from the wall ($y_{p+} = y_p u_\tau/\nu$) is also chosen to be 17.81. Thus the center of the sphere is in the buffer region and it is one diameter away from the wall.

The nondimensional height of the channel is 2. Along the spanwise direction periodic boundary conditions are employed and the spanwise extent of the computational domain is $4\pi/3$, which is the standard choice in turbulent channel flow simulations (Kim et al. 1987). Here we limit the streamwise extent of the computation domain to be 2.4, with upstream and downstream distances equal to 0.8 and 1.6. These upstream and downstream distances are 8 and 16 times the sphere diameter, and therefore can be considered more than adequate. A fully developed turbulent channel flow is applied as inflow at one streamwise end of the computational domain. A nonreflecting outflow boundary condition is applied at the other outflow end (Mittal and Balachandar 1996). These turbulent inflow simulations are similar in spirit to those in the context of freestream isotropic turbulence (Bagchi and Balachandar 2003, Bagchi and Balachandar 2004).

We use spectral element methodology (Deville et al. 2002), which offers both higher order accuracy and ability to construct complex boundary-fitted grid around the particles in a channel. These features are essential for reliable computations that are capable of capturing higher order turbulence statistics at high fidelity. The computational domain is partitioned into hexahedral elements, which are deformed by isoparametric mappings. Within each element, velocity and pressure are represented in local Cartesian coordinates by tensor-product Lagrange polynomials of degree N and $N-2$, respectively. Time stepping is based on semi-implicit splitting scheme that, with correct treatment of the incompressibility constraint, allows high-order temporal accuracy. The results to be reported here employ 3400 spectral elements with each element resolved by either $N = 9$ (higher resolution) or $N = 6$ (lower resolution) Lagrange Gauss-Lobatto points. Thus the effective grid size in the present simulations is 1.79 million points for $N = 9$ and 0.44 million points for $N = 6$.

An auxiliary single phase turbulent channel flow simulation (Kim et al. 1987) is performed alongside and the time-dependent velocity obtained from a streamwise plane is used as inflow for the spectral simulation with the particle. This auxiliary single phase simulation employs the standard Fourier-Fourier-Chebyshev spectral methodology in a box of nondimensional size $4\pi \times 2 \times 4\pi/3$ along the streamwise, wall-normal and spanwise directions. The resolution along these directions are $128 \times 128 \times 128$, which is quite adequate for the present case of $Re_\tau = 178.12$.

RESULTS

Resolution

A three-dimensional view of the spectral element grid is shown in figure 1a. Figure 1b shows the discretization on the streamwise wall-normal plane close to the sphere. Except within a small bounding box around the sphere, the spectral element grid is Cartesian in nature and the hexahedral elements are simply rectangular in shape. Within this bounding box the hexahedral elements deform from the outer box to the inner sphere.

The spectral element grid away from the sphere must be such that it should adequately resolve all the scales of turbulent channel flow. The region away from the sphere is discretized with 7, 20, and 22 spectral elements along the streamwise, wall-normal and spanwise directions. With $N = 9$ this yields effectively 57, 161 and 177 grid points along the three directions. In order to accommodate the bounding box the spectral elements are not of uniform width and furthermore the Gauss-Lobatto grid within the elements are nonuniformly distributed. With $N = 9$ the smallest and the largest grid spacings are 1.786 and 19.404 in wall units along the streamwise direction, 0.080 and 5.174 along the wall-normal direction and 1.071 and 6.663 along the spanwise direction. In comparison the discretization of the fully spectral channel flow simulation are 17.487 and 5.829 along the streamwise and spanwise directions, and along the wall-normal direction it varies from 0.054 to 4.371 from the channel wall to the centerline. The spectral element simulation simulation, although employs a larger number of grid points per computational volume than the corresponding fully spectral simulation, in terms of the largest grid spacing provides an equivalent fully spectral resolution of about $115 \times 105 \times 112$. Since the spectral element computation is fully dealiased, the above equivalent resolution is more than adequate for the present case of $Re_\tau = 178.12$ as will be demonstrated below.

First, we performed a turbulent channel inflow simulation in the absence of the sphere with the spectral element code. The grid resolution over the bulk of the channel was maintained the same as that for the simulation with the sphere. This will allow us to establish the adequacy of the spectral element grid in resolving all the scales of turbulent channel flow. In figure 2a we compare the mean streamwise velocity obtained from the spectral element simulation with that

of Kim et al. (1987), and the rms velocity fluctuations are shown in figures 2b, 2c and 2d. The results for the lower order ($N = 6$) spectral element simulation is also shown. The agreement in both the mean and the rms velocities is quite good indicating the adequacy of the present spectral element grid. In figure 3 we compare spanwise spectra of streamwise, wall-normal and spanwise velocities, obtained from the spectral element simulation with those from the fully spectral simulation. The comparisons are made at two different locations, one in the buffer region ($y_+ = 18.7$) and the other at the center of the channel ($y_+ = 178.12$). Comparison is good for the entire spectra indicating that all the turbulent scales are well resolved by the spectral element simulation.

The fully spectral simulation uses a periodic boundary condition along the streamwise direction with a long streamwise length. In contrast the spectral element simulation uses a shorter streamwise length with turbulent channel flow applied as inflow. In order to verify the appropriateness of this approach, the spanwise spectras shown in figure 3 were computed at different streamwise locations in the spectral element code and the results are remarkably similar indicating that the inflow turbulence is well maintained within the computed channel length.

The resolution around the sphere can be characterized as 384 surface elements and with $N = 9$ this yields a total of 202818 grid points around the sphere. Also the first grid point away from the surface of the sphere is at a radial distance of $\Delta r_+ = 0.089$. This choice of resolution close to the sphere has been guided by our prior experience with this code in solving wall-bounded flows over a sphere (Zeng et al. 2004). Based on sphere diameter and the mean turbulent velocity at the particle location we expect the mean particle Reynolds number to be about 210. Particle Reynolds number based on instantaneous velocity can be somewhat larger. The chosen grid around the sphere is more than adequate to resolve all the boundary layer dynamics around the sphere.

Drag and lift

In wall units the Kolmogorov length scale can be written in terms of local dissipation rate as $\eta_+ = \eta u_\tau/\nu = \epsilon_+^{-1/4}$. The dissipation rate increases monotonically from the center to the walls of the channel and accordingly the Kolmogorov length scale is the lowest ($\eta_+ = 1.55$) close to the wall and reaches a maximum at the channel centerline ($\eta_+ = 3.70$). Thus the sphere ($d_+ = 17.81$) ranges from 4.8 to 11.5 times the Kolmogorov scale.

First we consider the accuracy of the standard drag law in predicting the force on the sphere. The instantaneous nondimensional force on the sphere can be predicted as

$$\mathbf{F} = \frac{\mathbf{F}^*}{\rho H^2 u_\tau^2} = \frac{\pi}{8} C_D \frac{d_+^2}{Re_\tau^2} |\mathbf{u}_+| \mathbf{u}_+ \qquad (1)$$

where $\mathbf{u}_+ = \mathbf{u}^*/u_\tau$ is the undisturbed instantaneous velocity of the surrounding fluid evaluated at the center of the particle and since the sphere is stationary this is also the relative velocity of the fluid with respect to the particle. The drag coefficient is given in terms of particle Reynolds number as

$$C_D = \frac{24}{Re}\left(1 + 0.15 Re^{0.687}\right) \quad \text{where} \quad Re = \frac{|\mathbf{u}^*| d}{\nu} \qquad (2)$$

In the present case the undisturbed flow velocity at the center of the sphere can be unambiguously evaluated in the following way. The spectral element channel flow was simulated without the sphere in it, but with the same turbulent inflow as that with the sphere. The velocity from this sphere-free simulation measured at the location where the sphere would have been gives the undisturbed flow. Figure 4 shows the time history of all three components of the undisturbed flow velocity. Also plotted in figure 4 is the velocity magnitude, which resembles streamwise velocity since this is the dominant component of the flow.

Figure 5a shows the time history of the magnitude of force obtained from the direct numerical simulation for the case of $d_+ = 17.81$, $y_{p+} = 17.81$ with $N = 9$. For comparison, in figure 5a, also plotted is the force obtained using the standard drag relation (eqn 1). The streamwise, wall-normal and spanwise components of the actual DNS force and of the predicted force using the standard drag formula are plotted in figures 5b, 5c and 5d. As expected the force is dominated by the streamwise component and the large scale up and down oscillations are reasonably well predicted by the standard drag relation. However, there is significant over-prediction of the amplitude of such oscillations and also there are differences in the high frequency component. From figure 4 it is also clear that these large scale oscillations in the force are directly associated with the change in the undisturbed fluid flow that the sphere sees. The spanwise component of the force is smaller in magnitude and its correspondence to that predicted by the standard drag relation is similar to the behavior of the streamwise component. The wall-normal force is the smallest and it is in agreement with the smaller magnitude of the wall-normal component of the undisturbed fluid velocity. Unlike the other two components, the computed wall-normal force differs from the prediction even in the mean value.

The mean and rms of the magnitude as well as the components are shown in table 1 for both the actual and the predicted force. The mean value of the streamwise and spanwise forces are well predicted by the standard drag relation. This behavior is similar to that observed for the case of isotropic turbulent flow over a sphere (Bagchi and Balachandar 2003). The effect of the bounding wall is thus minimal, at least at a distance of $y_{p+} = 17.81$. In contrast, the mean value of the predicted wall-normal force is small and positive, while the mean computed wall-normal force is about an order of magnitude larger than predicted and is directed towards the wall. The Reynolds number of the flow around the sphere is about 210 and at this Re the shear induced lift coefficient is negative and thus may at least partly account for the difference. As shown in the table, while the streamwise fluctuations are over-predicted by the standard drag relation, the fluctuation in the other two components are somewhat under-predicted. This may be improved with the inclusion of shear induced lift force.

In future we plan to include added-mass, Basset history and shear lift components to the prediction and investigate their influence on predictive capability. We will also extend the present study to include spheres of varying sizes and also place the spheres at locations other than the buffer layer.

REFERENCES

Bagchi, P. and Balachandar, S., 2003, "Effect of turbulence on the drag and lift of a particle", *Physics of Fluids*, Vol. 15, pp. 3496-3513.

Bagchi, P. and Balachandar, S., 2004, "Response of the

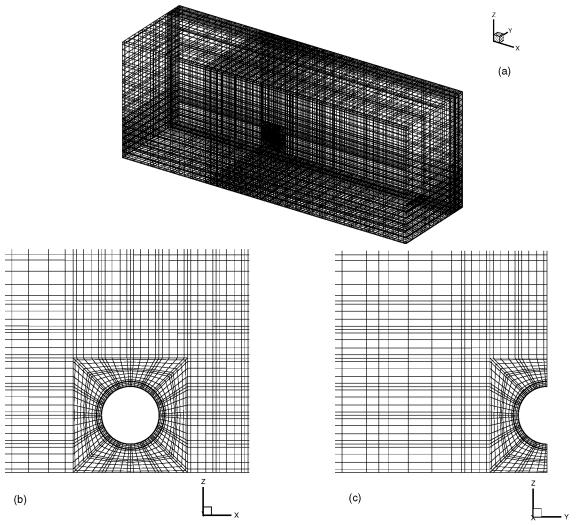

Figure 1: Sample spectral element discretization of the computational domain for the $L = 1$ case. (a) The entire computational domain; (b) zoom-up of the discretization near the sphere on the x-z plane; (c) zoom-up of the discretization near the sphere on the y-z plane.

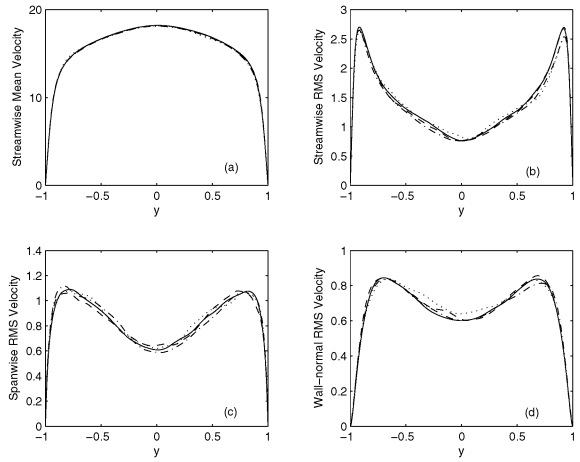

Figure 2: Velocity profiles along wall-normal directions. (a) streamwise mean; (b) streamwise RMS; (c) spanwise RMS; (d) wall-normal RMS. —: channel with spectral element method for N=9; $-\cdot-$: channel with spectral element method for N=6; - -: fully spectral channel for ny=128; $\cdots$: fully spectral channel for ny=64.

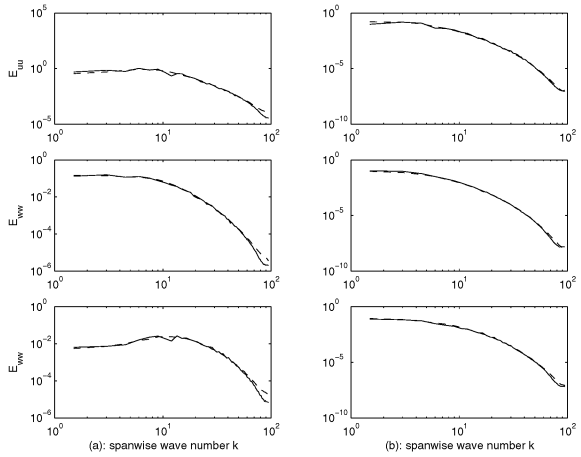

Figure 3: Spanwise spectra of streamwise, spanwise, and wall-normal velocities. (a) —: channel with spectral element method for N=9 at $y_+ = 18.7$, - -: fully spectral channel for ny=128 at $y_+ = 19.02$; (b) —: channel with spectral element method for N=9 at $y_+ = 178.12$, - -: fully spectral channel for ny=128 at $y_+ = 178.12$.

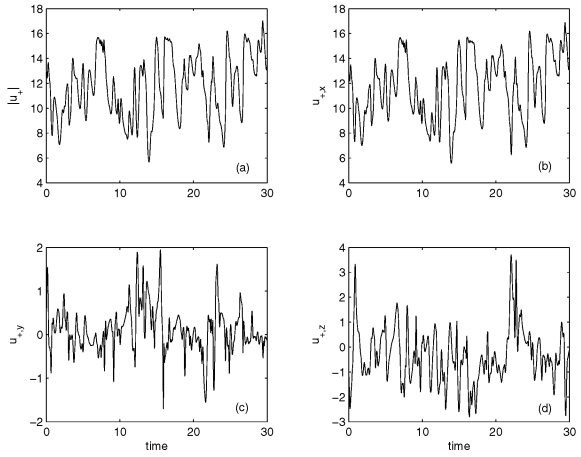

Figure 4: Time history of the velocities at the sphere location with the absence of the sphere. (a) magnitude of the velocity; (b) streamwise velocity; (c) wall-normal velocity; (d) spanwise velocity.

wake of an isolated particle to an isotropic turbulent flow", *Journal of Fluid Mechanics*, Vol. 518, pp. 95-123.

Brucato, A., Grisafi, F., and Montante, G., 1988, "Particle drag coefficients in turbulent fluids", *Chemical Engineering Science*, Vol. 53, pp. 3295-3314.

Crowe, C. T., Sommerfeld, M., and Tsuji, Y., 1988, "Multiphase flows with droplets and particles ", CRC Press, New York.

Dandy, D. S. and Dwyer, H. A., 1990, "A sphere in shear flow at finite Reynolds number: effect of shear on particle lift, drag and heat transfer", *Journal of Fluid Mechanics*, Vol. 216, pp. 381-410.

Deville, M. O., Fischer, P. F., and Mund, E. H., 2002, "High-order methods for incompressible fluid flow", Cambridge University Press, New York.

Fessler, J. R., Kulick, J. D., and Eaton, J. K., 1994, "Preferential concentration of heavy particles in a turbulent channel flow", *Physics of Fluids*, Vol. 6, pp. 3742-3749.

Gore, R. A. and Crowe, C. T., 1990, "Discussion of particle drag in a dilute turbulent two-phase suspension flow", *International Journal of Multiphase Flow*, Vol. 16, pp. 359-361.

Kaftori, D., Hetsroni, G., and Banerjee, S., 1995, "Particle behavior in the turbulent boundary layer: I. Motion, deposition and entrainment", *Physics of Fluids*, Vol. 7, pp. 1095-1106.

Kim, J., Moin, P., and Moser, R. D., 1987, "Turbulence statistics in fully developed channel flow at low Reynolds number", *Journal of Fluid Mechanics*, Vol. 177, pp. 133-166.

Mei, R., 1992, "An approximate expression for the shear

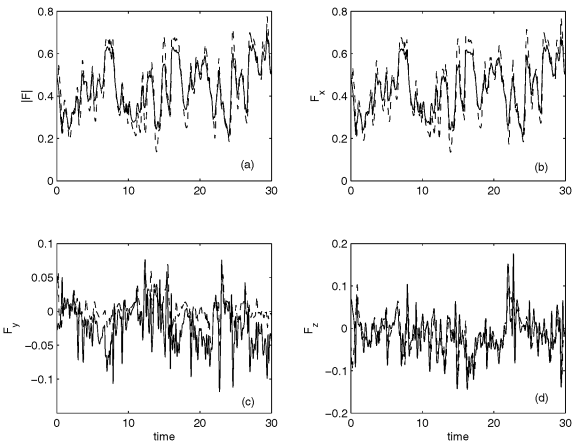

Figure 5: Time history of the forces. (a) magnitude of the force; (b) streamwise force; (c) wall-normal force; (d) spanwise force. —: present DNS results; - -: predicted forces using standard drag formulation.

Table 1: Mean and RMS of the forces.

	$N = 9$		$N = 6$	
	present	predicted	present	predicted
$\overline{\lvert\mathbf{F}\rvert}$	0.4395	0.4395	0.4692	0.4804
$\overline{\mathbf{F_x}}$	0.4356	0.4370	0.4643	0.4777
$\overline{\mathbf{F_y}}$	-0.0214	0.0031	-0.0269	-0.0019
$\overline{\mathbf{F_z}}$	-0.0141	-0.0140	-6.7877e-04	-0.0016
$\lvert\mathbf{F}\rvert'$	0.1119	0.1444	0.0966	0.1344
$\mathbf{F_x'}$	0.1111	0.1445	0.0950	0.1345
$\mathbf{F_y'}$	0.0314	0.0181	0.0315	0.0211
$\mathbf{F_z'}$	0.0442	0.0397	0.0566	0.0453

lift force on a spherical particle at finite Reynolds number", *International Journal of Multiphase Flow*, Vol. 18, pp. 145-147.

Mittal, R. and Balachandar, S., 1996, "Direct numerical simulation of flow past elliptic cylinders", *Journal of Computational Physics*, Vol. 124, pp. 351-367.

Ranz, W. E. and Marshall, W. R., 1952, "Evaporation from drops", *Chemical Engineering Progress*, Vol. 48, pp. 141-146.

Schiller, L. and Naumann, A., 1933, "Uber die grundlegenden berechungen bei der schwerkraftaufberereitung", *Zeitschrift Des Vereines Deutscher Ingenieure*, Vol 77, pp. 318-320.

Sirignano, W. A., 1999, "Fluid dynamics and transport of droplets and sprays ", Cambridge University Press, New York.

Tsuji, Y. and Morikawa, Y., 1982, "LDV measurements of an air-solid two-phase flow in a horizontal pipe", *Journal of Fluid Mechanics*, Vol. 120, pp. 385-409.

Wu, J. S. and Faeth, G. M., 1994a, "Sphere wakes at moderate Reynolds numbers in a turbulent environment", *AIAA Journal*, Vol. 32, pp. 535-541.

Young, J. B. and Hanratty, T. J., 1991, "Optical studies on the turbulent motion of solid particles in a pipe flow", *Journal of Fluid Mechanics*, Vol. 231, pp. 665-688.

Zeng, L., Balachandar, S., and Fischer, P., 2004, "Wall-induced forces on a rigid sphere at finite Re", submitted to